2021 IEEE 32nd Annual International Symposium on Personal, Indoor and Mobile Radio Communications (PIMRC) | 978-1-7281-7586-7/21/$31.00 ©2021 IEEE | DOI: 10.1109/PIMRC50174.2021.9569533

# UAV Deployment for Throughput Maximization in a UAV-Assisted Cellular Communications

Nishant Gupta[1], Satyam Agarwal[1], and Deepak Mishra[2]

[1]Department of Electrical Engineering, Indian Institute of Technology Ropar, Punjab, India
[2]School for Electrical Engineering and Telecommunications, University of New South Wales, Sydney, Australia
E-mails: 2018eez0018@iitrpr.ac.in, satyam6099@gmail.com, dph.mishra@gmail.com

***Abstract*—Unmanned Aerial Vehicle (UAV) deployment as an aerial base station in fifth-generation (5G) communication system has emerged as a promising technology to provide seamless communication in a geographical region. The UAV's high mobility potential offers additional degrees of freedom for effective deployment. Therefore, the three-dimensional (3D) deployment of UAV is one of the key challenges in UAV-assisted communication systems. In this paper, we address the problem of UAV deployment in 3D space to provide on-demand coverage to the ground users to maximize the sum rate. We consider realistic UAV-ground channel model derived from extensive experiments. The problem formulated is non-convex. To obtain the optimal location, we approximate the rate expression to identify the concave regions and propose a low-complexity solution by applying alternating optimization. Through simulation results, we provide valuable insights into the low-complexity solution.**

***Index Terms*—UAV deployment, 3D-placement, fifth-generation (5G), throughput maximization, on-demand coverage**

## I. Introduction

The growing demand for a higher data rate has placed a massive challenge for the traditional cellular network. Most studies have explored the utilization of unlicensed spectrum, equipping multiple antennas at the base station (BS), etc., for increasing network capacity. However, these techniques have failed when the channel between the BS and the user is weak or when a significant number of users are present in a given area with overwhelming data requirements [1].

Unmanned aerial vehicles (UAVs) have emerged as a promising technology to provide wireless coverage to a geographical region. Owing to their aerial nature, UAVs can maintain a line-of-sight (LoS) connection with the ground users resulting in improved coverage and performance. Therefore, it is desirable to use the UAVs as an aerial node to enhance wireless services and coverage in hotspot areas, such as football stadiums, public services, fire-fighting, etc. [2].

In this work, we focus on UAV-assisted cellular networks where UAV acts as an aerial BS to offload some traffic from the existing cellular network, such as in a sports stadium, live concerts, etc. The three-dimensional (3D) placement of UAV is one of the key challenges in UAV-assisted communication systems. Being mobile, UAVs can adjust their position flexibly on-demand as compared to the conventional BS and offer effective performance. In particular, optimal deployment is a crucial design factor when using UAV for on-demand coverage, Internet-of-things applications, etc. [3]. The 3D deployment of UAV is a difficult task since it relies on the locations of the ground users and the channel characteristics of UAV-to-ground user links, which is also a function of UAV's altitude. Therefore, it is crucial to obtain the deployment location of UAVs to enhance system performance.

### A. State-of-the-Art

Optimal deployment of UAVs to enhance system performance has gained considerable attention and has been an active area of research in recent years. Researchers have focused on finding the optimal UAV placement, where the UAVs act as an aerial quasi-static BS to support ground users in a given area or to maximize the coverage area [4]–[9]. In [5], the authors optimized the UAV altitude to provide maximum coverage to the ground users. In contrast, the UAV horizontal location was optimized in [6] by fixing its height to minimize the number of UAVs required to provide coverage in a given area. In 3D space, the issue of a drone-enabled small cell placement optimization was explored in [7] to maximize the number of users served. In [8], and [9], a similar objective was considered in the presence of the minimum rate requirement for each user.

Some works [10]–[12] focused on UAV deployment with an objective to maximize rate. The authors in [10] maximized the communication rate by optimizing the UAV's altitude and antenna beamwidth. In [11], the authors maximized the sum rate in the presence of a constant-modulus constraint for the beamforming vector in millimeter-wave communications. However, in their work, the authors fixed the altitude of the UAV. Multi-UAV deployment problem was also investigated in [12] by maximizing the minimum rate for all ground users while assuming the channel to be dominated by LoS links.

### B. Motivation and Contributions

Towards this direction, our current work bridges the gap in the existing literature by finding an optimal deployment location for UAV in 3D space where the sum-rate over all ground users is maximized while considering a realistic UAV-user channel model. UAV-user channel is modelled as LoS and non-LoS (NLoS) components as obtained from practical experiments [13]. This scenario is relevant to many applications where the deployment location of UAV is unknown and is dependent on the ground users and air-to-ground channel

characteristics. For example, in providing high rates to the audience in a football stadium or to the first responders in emergencies. The key contributions of this paper are as follows:

- We formulate a 3D deployment problem that computes the optimal location for UAV deployment in 3D space by maximizing the sum rate over all users.
- Realistic channel model based on extensive experimental study has been incorporated to obtain a better UAV deployment location.
- The problem formulated is non-convex and NP-hard. As a result, a closed-form approximation of rate expression is provided, and conditional concavity is explored to achieve a low-complexity solution for 3D deployment problem.
- Finally, numerical results provide useful insights into the optimal deployment location. The effectiveness of the proposed approach to obtain the optimal location is shown.

## II. System Model and Problem Definition

Consider a system consisting of $N$ users, indexed by $\mathcal{N} \triangleq \{1, \cdots, N\}$, distributed randomly in a circular field of radius $r$. The users are static, and the location of $i^{th}$-user is given by $(\mathcal{U}_i, 0)$, where $\mathcal{U}_i = [x_i, y_i] \in \mathbb{R}^{1\times 2}$, where $i \in \mathcal{N}$, and $\mathbb{R}$ denotes the set of real-valued numbers. A downlink communication setup is considered, where the UAV serves the $N$ ground users using frequency division multiple access (FDMA) as the channel access technique. Under this FDMA scheme, we assume that the UAV allocates equal channel bandwidth to each mobile ground user to maintain fairness and avoid interference. To serve them, we deploy a single UAV at the optimal location. The optimal location is the location of the UAV in 3D space where the sum rate over all ground users is maximum.

Air-to-ground signal transmission is affected by environmental barriers, such as obstacles, buildings, etc. Depending upon the environment, the air-to-ground propagation channel can be modelled by either the LoS or NLoS components. However, while analysing the UAV-based communication system, a detailed description about the location and height of the obstacles might not be available [13]. Therefore, we model the air-to-ground propagation channel by jointly considering the LoS and NLoS components along with their occurrence probabilities separately [14]. Then, the path loss for LoS and NLoS links are expressed as

$$\begin{aligned} L_L^i &= d_0 d_i^{-\bar{\alpha}}, \text{ for LoS link, and} \\ L_N^i &= \kappa d_0 d_i^{-\bar{\alpha}}, \text{for NLoS link.} \end{aligned} \tag{1}$$

Here $d_0$ represents the path loss at a reference distance of 1 m, $d_i$ is the distance between the UAV and the $i^{th}$-user and is given by $d_i = \sqrt{(x-x_i)^2 + (y-y_i)^2 + z^2}$, where $(x, y, z)$ denote the UAV's location. $\bar{\alpha}$ represents the path loss exponent, and $\kappa < 1$ accounts for the additional attenuation factor.

The probability of having LoS for $i^{th}$-user depends upon the elevation angle between the UAV and the $i^{th}$-user [5]. This LoS probability is given by

$$P_{LoS}(\phi_i) = 1/(1 + C\exp(-D[\phi_i - C])), \tag{2}$$

where $C$ and $D$ are parameters depending on the environment, such as suburban, urban, dense urban, etc. $\phi_i$ (in degrees) is the elevation angle of UAV from the $i^{th}$-user and is given by $\phi_i = \frac{180}{\pi}\sin^{-1}\left(\frac{z}{d_i}\right)$. Then, the corresponding NLoS probability can be obtained as $P_{NLoS}(\phi_i) = 1 - P_{LoS}(\phi_i)$. Therefore, the average path loss $g_i$ between the UAV and the $i^{th}$-user can be expressed as

$$g_i = P_{LoS}(\phi_i)L_L^i + P_{NLoS}(\phi_i)L_N^i = \widehat{P}_{LoS}(\phi_i) d_0 d_i^{-\bar{\alpha}}, \tag{3}$$

where $\widehat{P}_{LoS}(\phi_i) = (1-\kappa)P_{LoS}(\phi_i) + \kappa$.

Let $P_{tr}$ denote the UAV transmit power. The achievable rate in bits/second (bps) between the UAV and the $i^{th}$-user is given by [15, Eq. 10],

$$R_i = \frac{B}{N}\log_2\left(1 + \frac{P_{tr} g_i}{\sigma^2}\right), \tag{4}$$

where $B$ denotes the total channel bandwidth, and $\sigma^2$ is the channel noise power at the receiver. Substituting (3) in (4), we get

$$R_i = \frac{B}{N}\log_2\left(1 + \frac{\tilde{\gamma}_o \widehat{P}_{LoS}(\phi_i)}{((x-x_i)^2 + (y-y_i)^2 + z^2)^{\alpha}}\right), \tag{5}$$

where $\tilde{\gamma}_o \triangleq P_{tr} d_0/\sigma^2$, and $\alpha \triangleq \bar{\alpha}/2$.

Our objective in this paper is to provide an on-demand coverage to the ground users by deploying the UAV at an optimal location in 3D space to achieve the best performance. In other words, given a circular field with $N$ users, what is the optimal location in 3D space where the UAV should be deployed to maximize the sum rate capacity?

The sum rate maximization problem is formulated as

$$\begin{aligned} \text{(P1)}: \max_{\{x,y,z\}} \quad & Q \triangleq \sum_{i=1}^{N} R_i \\ \text{subject to (s.t.)}: \; & -r \le x, y \le r; H \le z \le H_{max}, \end{aligned}$$

where $H$ is the minimum height required by the UAV to avoid ground obstacles and make horizontal movements, and $H_{max}$ is the maximum height achievable by the UAV. Since all the users are present in the circular field of radius $r$ centered at origin, then it can be easily interpreted that the optimal values of $x$ and $y$ will also lie in the circular field. Therefore, we restrict the search space of $x$ and $y$ to the radius of circular field *i.e.,* $-r \le x, y \le r$. Next, we obtain the solution to (P1).

## III. Optimal UAV 3D-Location

In this section, we obtain the solution to problem (P1). $R_i$ defined in (5) is a function of not only the distance between the UAV and the $i^{th}$-user but also $\widehat{P}_{LoS}(\phi_i)$, which makes $R_i$ difficult to handle. $R_i$ defined in (5) is a non-concave function, hence it is difficult to obtain the optimal solution of

(P1). Exhaustive search (ES) can be used to obtain the global solution, albeit with a high computational complexity. From the problem (P1), we analyzed that for specific ranges of $x$, $y$, and $z$, the function is concave if the variable $(x, y, \text{or } z)$ is taken individually. Thus to have a faster solution, we exploit this unique feature of the objective function in the next sub-section to find the concave regions. In the following, we break the domain of the function under individual variable $(x, y, \text{ or } z)$ into two parts, concave and non-concave. In the concave, we can apply faster search algorithms like golden section search (GSS) [16], whereas in the non-concave region we can use linear search to find the maxima in the specified interval.

Thereafter, we use an alternating maximization to solve (P1) where the objective function over the single variable is maximized using the combination of GSS and linear search.

In general, it is difficult to evaluate the closed-form expression for the region where the sum rate $Q \triangleq \sum_{i=1}^{N} R_i$ is concave. Thus, to get analytical insights on the concavity, we approximate the sigmoidal function in $\widehat{P}_{LoS}(\phi_i)$ described in (2) and (3) to obtain a closed-form approximation for the concave region in $Q$. Thereafter, for individual maximization over a concave domain, GSS is used which reduces the computations significantly.

### A. Approximation and Concave Regions

We provide an approximation to the sigmoidal function defined in the expression of $R_i$. We propose two approximations to $R_i$, namely step and linear as discussed below.

*1) Step Approximation:* For higher values of $D$, *i.e.,* $D \gg 1$ and sufficient UAV height in (2), $P_{LoS}(\phi_i)$ tends to one *i.e.,* $P_{LoS}(\phi_i) \approx 1, \forall i \in \mathcal{N}$. The approximate $R_i$ is given as

$$\widetilde{R}_i^S = \frac{B}{N} \log_2 \left( 1 + \frac{\tilde{\gamma}_o}{((x - x_i)^2 + (y - y_i)^2 + z^2)^{\alpha}} \right). \quad (6)$$

$\widetilde{R}_i^S$ defined above is still a non-concave function of $x$, $y$, and $z$. However, we can obtain the domain over which the function is concave in $x$, $y$, and $z$ individually.

*Lemma 1:* The region over which $\widetilde{Q}^S \triangleq \sum_{i=1}^{N} \widetilde{R}_i^S$ is individually concave in $x$, $y$, and $z$ is given by $\mathcal{R}_x^S$, $\mathcal{R}_y^S$, and $\mathcal{R}_z^S$, respectively, in (A.7), where $\widetilde{R}_i^S$ is defined in (6).

*Proof:* See Appendix A. ∎

*2) Linear Approximation:* If the value of $D$ is small, *i.e.,* $D \ll 1$ in (2), then the sigmoidal function in (2) can be approximated as $\frac{z}{\sqrt{(x-x_i)^2+(y-y_i)^2+z^2}}$. Then, $R_i$ defined in (5) is approximated as

$$\widetilde{R}_i^L = \frac{B}{N} \log_2 \left( 1 + \tilde{\gamma}_o \frac{\frac{(1-\kappa)z}{\sqrt{(x-x_i)^2+(y-y_i)^2+z^2}} + \kappa}{((x - x_i)^2 + (y - y_i)^2 + z^2)^{\alpha}} \right). \quad (7)$$

Again, $\widetilde{R}_i^L$ in (7) is non-concave with respect to $x$, $y$, and $z$. Next, we present a lemma to find the region of individual concavity of $\widetilde{Q}^L \triangleq \sum_{i=1}^{N} \widetilde{R}_i^L$ in $x$, $y$, and $z$.

*Lemma 2:* $\widetilde{Q}^L \triangleq \sum_{i=1}^{N} \widetilde{R}_i^L$ defined above is individually concave with respect to $x$, $y$, and $z$ in the region defined by $\mathcal{R}_x^L$, $\mathcal{R}_y^L$, and $\mathcal{R}_z^L$ given in (B.7), respectively.

*Proof:* See Appendix B. ∎

From Lemmas 1 and 2, we obtained the regions where $\widetilde{Q}$ is concave in $x$, $y$, and $z$, individually, using step or linear approximations, respectively. Note that $\widetilde{Q} = \widetilde{Q}^S$ if $D \gg 1$ and $\widetilde{Q} = \widetilde{Q}^L$ if $D \ll 1$.

### B. Solution Using Alternating Optimization

Alternating optimization (AO) is employed to obtain a sub-optimal solution of (P1). In AO, the function is maximized over a single variable successively and the algorithm iterates to obtain a sub-optimal solution. While optimizing the function over a single variable $x$, $y$ or $z$, the domain of the function is divided into two parts: concave and non-concave. Over the concave region 1D-GSS is used while in the non-concave region linear search is employed. The individually concave regions are defined as $\mathcal{R}_\psi$, $\psi \in \{x, y, z\}$ that are obtained either using the step or linear approximation. Let $\mathcal{B}_x$, $\mathcal{B}_y$, and $\mathcal{B}_z$ be the region spanned by $-r \leq x \leq r$, $-r \leq y \leq r$, and $H \leq z \leq H_{max}$ for $x$, $y$, and $z$, respectively. Then, the non-concave regions are given by $\mathcal{B}_\psi \backslash \mathcal{R}_\psi$.

The algorithm repetitively gives the alternating individual optimization sequence of $x_k$, $y_k$ and $z_k$ at the $k^{th}$ iteration. $Q_k$ is the sum rate at the $k^{th}$ iteration. The algorithm iterates until $|Q_k - Q_{k-1}| \geq \epsilon$, where $\epsilon$ is the acceptable tolerance threshold. In each alternating maximization subproblem, we obtain two solutions, one corresponding to the GSS applied over concave region and second corresponding to the linear search over non-concave region. The best among the two is chosen as the solution to the alternating maximization subproblem. The steps to obtain the sub-optimal solution of (P1) is presented in Algorithm 1. Later, in the numerical section, it is observed that the sub-optimal solution obtained by using this low complexity algorithm is very close to the globally optimal solution obtained using ES. The solution obtained for (P1) is named as $\mathcal{X}^* = (x^*, y^*, z^*)$.

**Algorithm 1** AO to obtain sub-optimal solution of (P1)

**Input:** $r$, $H$, $H_{max}$, $\mathcal{B}_x$, $\mathcal{B}_y$, $\mathcal{B}_z$, $N$, $(x_i, y_i), \forall i \in \mathcal{N}$ and $\epsilon$.
**Output:** $Q^*$ along with $\mathcal{X}^* = (x^*, y^*, z^*)$.
1: Initialize $k = 1$, $y = -r$, $z = H$, $Q_0 = 0$, and $Q_1 = 0.1$.
2: Calculate $\mathcal{R}_x$, $\mathcal{R}_y$, and $\mathcal{R}_z$, obtained either by step or linear approximation using (A.7) or (B.7), respectively.
3: **while** $Q_k - Q_{k-1} \geq \epsilon$ **do**
4: $k = k + 1$.
5: **for** $\psi \in \{x, y, z\}$ **do**
6: For $\mathcal{R}_\psi$, compute $\psi_1^* = arg \max_{\psi} Q \triangleq \sum_{i=1}^{N} R_i$, using 1D GSS within acceptable tolerance $\epsilon$.
7: Evaluate $\psi_2^* = arg \max_{\psi} Q$, through linear search with step size $\epsilon$ by varying $\psi$ over the region $\mathcal{B}_\psi \backslash \mathcal{R}_\psi$.
8: Find $\psi^* = arg \max_{\{\psi_j^*\}} Q$ for $j \in \{1, 2\}$.
9: Substitute $\psi = \psi^*$ in $Q$.
10: Set $Q_k = Q$.
11: Set $Q^* = Q_k$.

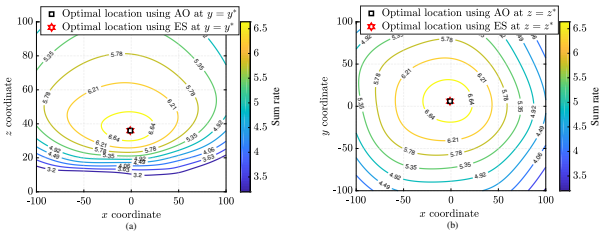


Fig. 1. Validation of optimal location at (a) $y = y^*_{es}$, (b) $z = z^*_{es}$. AO and ES are the alternating optimization and exhaustive search, respectively.

### C. Convergence and Complexity

Since (P1) is a non-convex problem, we used AO to obtain the deployment location of UAV by applying 1D GSS in the concave region and linear search in the non-concave region. The number of iterations involved in the convergence of AO is as follows. In each iteration for concave region, the search space $\Delta x = (x^{ub} - x^{lb})$, $\Delta y = (y^{ub} - y^{lb})$, and $\Delta z = (z^{ub} - z^{lb})$ reduces by a factor of 0.618 [16]. $\psi^{ub}$ and $\psi^{lb}$ denote the upper and lower bound of the concave region in the search space, respectively, that are computed either by using (A.7) or (B.7), where $\psi \in \{x, y, z\}$. Let $N_\psi = \frac{\psi^{ub} - \psi^{lb}}{\epsilon}$, $\psi \in \{x, y, z\}$, denote the number of computations to find maximum sum rate in $\psi$ in the non-concave region. Then, the average number of iterations are given by $N_{itr} = 2N_p \left( \ln\left(\frac{\Delta x}{\epsilon}\right) + \ln\left(\frac{\Delta y}{\epsilon}\right) + \ln\left(\frac{\Delta z}{\epsilon}\right) + N_x + N_y + N_z \right)$, where $N_p$ denotes the number of executions of the main loop in Algorithm 1. The term in parenthesis are the number of iterations involved to obtain the optimal value for each variable in concave and non-concave region. The worst-case number of iterations of (P1) in AO when no concave regions are found is $N_{itr} = N_p(N_x + N_y + N_z)$.

Whereas using ES, the total computations taken to find the optimal location with maximum sum rate is $N_x N_y N_z$.

## IV. Results and Discussion

In this section, numerical results are provided to validate the performance of the proposed deployment scheme. We consider a system with 10 users [17] that are distributed randomly in a circular field of radius 150 m, centered at origin. The total communication bandwidth $B$ is set to 1 MHz. The reference SNR at distance $d_0 = 1$ m is taken as $\tilde{\gamma}_o = 80$ dB. The modelling parameters are set as $C = 10$, $D$ = 0.6, $\kappa = 0.2$, and $\bar{\alpha} = 2.3$ [15]. The $H$ to be attained by the UAV is set to 15 m. The acceptable tolerance is taken as $\epsilon = 1 \times 10^{-6}$.

To validate the optimal location for UAV deployment we plot Fig. 1. The solution using ES is $(x^*_{es}, y^*_{es}, z^*_{es})$. In Figs. 1(a) and (b), contour lines for sum rate is plotted against $x$ and $z$ for a given $y = y^*_{es}$, and $x$ and $y$ for a given $z = z^*_{es}$, respectively. The figure also shows that the low-complexity solution obtained using AO for problem (P1) converges to the solution obtained by using ES. On performing simulations on Intel Core $i7$ processor with 3.20 GHz CPU clock, the solution obtained using AO is twelve times faster than that obtained using ES. Thus, we infer that the proposed AO strategy provides a better complexity compared to ES.

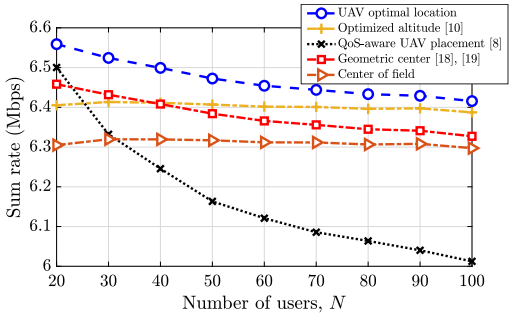


Fig. 2. Variation of sum rate at optimal location with other schemes by varying number of users $N$.

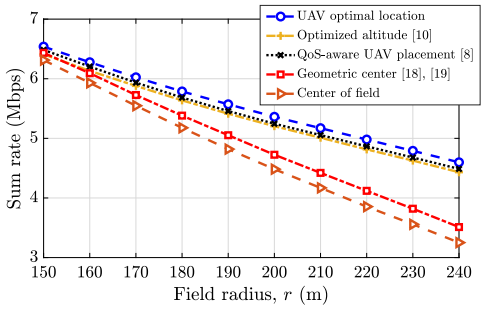


Fig. 3. Variation of sum rate at optimal location with other schemes by varying field radius $r$.

To show the effectiveness of the proposed strategy, we compare the sum rate of proposed solution with optimized altitude [10], QoS-aware UAV placement [8], geometric center [18], [19], and center of the field. In optimized altitude, the UAV altitude is optimized to obtain a maximum sum rate of the system while fixing the horizontal coordinates to the center of the field. QoS-aware UAV placement finds the 3D placement of UAV by considering the different QoS requirements of the ground users to maximize the achievable sum rate. In geometric center, the horizontal location of the UAV is set to the geometric center of all users. Whereas in center of the field case, the horizontal location is set to the center of the field while the UAV altitude is set to 25 m for both schemes.

Fig. 2 shows the sum rate comparison of the proposed scheme with different schemes as addressed above and is plotted by varying the number of users in a circular field of radius $r = 150$ m. It is observed that the sum rate of the optimal location is higher than the other schemes. It is because the proposed scheme jointly optimizes the horizontal and vertical coordinates of the UAV. In contrast, the other schemes either optimize the UAV altitude or considers fixed altitude. Also, a sharp decrease in the QoS-aware UAV placement scheme is observed because the QoS-based scheme focuses on rate fairness rather than maximizing the average sum rate.

Fig. 3 is plotted for $N = 20$ users by varying the radius of the circular field. As the field radius $r$ increases, the path loss increases. Thus, the sum rate decreases with an increase in the field radius. Here the performance of QoS-aware UAV placement is better than other schemes due to the fixed number of users in a field. Intuitively, the optimal UAV height should

increase with an increase in the field radius. Due to fixed UAV height in the geometric center and the center of the field cases, the sum rate worsens with an increase in the field radius. As a result, it gives a lower sum rate in comparison to others.

## V. Conclusion

This paper studies the UAV deployment location to maximize the sum rate of the UAV-assisted cellular communications. The rate expression is non-concave and is approximated to obtain closed-form expression for the concave regions. The optimal location for UAV deployment was obtained by using the alternating maximization. It utilized GSS in the concave region and linear search in the non-concave region. Results show that the optimal location obtained using alternating maximization yielded a low-complexity solution while providing solution close to the globally optimal solution. Simulation results show our proposed strategy outperforms the sum rate obtained by using benchmark schemes. Future extensions include UAV trajectory design to reach the deployment location by considering the energy requirements.

## Appendix A
## Proof of Lemma 1

We know $\widetilde{R}_i^S = \frac{B}{N}\log_2(1+S_i^S)$, where $S_i^S = \frac{\tilde{\gamma}_o}{((x-x_i)^2+(y-y_i)^2+z^2)^\alpha}$. Since logarithm $\log_2(.)$ preserves the concavity [20], the concave region of $\widetilde{R}_i^S$ is equivalent to $S_i^S$. The double derivative of $S_i^S$ is given by

$$\frac{\partial^2 S_i^S}{\partial x^2} = \mathcal{A}_2\left((2\alpha+1)(x-x_i)^2-(y-y_i)^2-z^2\right), \quad \text{(A.1)}$$

$$\frac{\partial^2 S_i^S}{\partial y^2} = \mathcal{A}_2\left((2\alpha+1)(y-y_i)^2-(x-x_i)^2-z^2\right), \quad \text{(A.2)}$$

$$\frac{\partial^2 S_i^S}{\partial z^2} = \mathcal{A}_2\big(2\alpha z^2-x^2+2xx_i-x_i^2-y^2+2yy_i-y_i^2+z^2\big). \quad \text{(A.3)}$$

where $\mathcal{A}_2 = 2\alpha\tilde{\gamma}_o\mathcal{A}_1^{-\alpha-2}$, and $\mathcal{A}_1 = (x-x_i)^2+(y-y_i)^2+z^2$. On solving for $\{\frac{\partial^2 S_i^S}{\partial x^2}, \frac{\partial^2 S_i^S}{\partial y^2}, \frac{\partial^2 S_i^S}{\partial z^2}\} \le 0$, we obtain the regions as $\mathcal{R}_{xs}^i$, $\mathcal{R}_{ys}^i$, and $\mathcal{R}_{zs}^i$ defined by $x \in (x_i^{lb}, x_i^{ub})$ given $(y,z)$, $y \in (y_i^{lb}, y_i^{ub})$ given $(x,z)$, and $z \in (z_i^{lb}, z_i^{ub})$ given $(x,y)$, respectively, where the function is individually concave. $\psi_i^{lb}$ and $\psi_i^{ub}$ denote the lower and upper bounds of $\psi$ for $i^{th}$-user, respectively, where $\psi \in \{x,y,z\}$ and are given by

$$\{x_i^{lb}, x_i^{ub}\} = \frac{1}{2\alpha+1}\Bigg(\alpha x_i \pm \big(2\alpha y^2 - 4\alpha y y_i + 2\alpha y_i^2 + 2\alpha z^2 + y^2 - 2yy_i + y_i^2 + z^2\big)^{-\frac{1}{2}} + x_i\Bigg), \quad \text{(A.4)}$$

$$\{y_i^{lb}, y_i^{ub}\} = \frac{1}{2\alpha+1}\Bigg(\alpha y_i \pm \big(2\alpha x^2 - 4\alpha x x_i + 2\alpha x_i^2 + 2\alpha z^2 + x^2 - 2xx_i + x_i^2 + z^2\big)^{-\frac{1}{2}} + y_i\Bigg), \quad \text{(A.5)}$$

$$\{z_i^{lb}, z_i^{ub}\} = \pm\frac{\sqrt{x^2-2xx_i+x_i^2+y^2-2yy_i+y_i^2}}{\sqrt{2\alpha+1}}. \quad \text{(A.6)}$$

Then, for $N$ users, we obtain $N$ regions corresponding to each user where the function is concave in either $x$, $y$ or $z$. The overall individual concave region is given by

$$\mathcal{R}_x^S = \bigcap_{i=1}^N \mathcal{R}_{xs}^i, \mathcal{R}_y^S = \bigcap_{i=1}^N \mathcal{R}_{ys}^i, \text{ and } \mathcal{R}_z^S = \bigcap_{i=1}^N \mathcal{R}_{zs}^i. \quad \text{(A.7)}$$

Hence, $\widetilde{Q}^S$ is concave with respect to $x$, $y$, and $z$, individually, in the region $\mathcal{R}_x^S$, $\mathcal{R}_y^S$, and $\mathcal{R}_z^S$, respectively.

## Appendix B
## Proof of Lemma 2

We know $\widetilde{R}_i^L = \frac{B}{N}\log_2(1+\tilde{\gamma}_o S_i^L)$, where $S_i^L = \frac{\frac{(1-\kappa)z}{\sqrt{(x-x_i)^2+(y-y_i)^2+z^2}}+\kappa}{((x-x_i)^2+(y-y_i)^2+z^2)^\alpha}$. Since logarithm $\log_2(.)$ preserves concavity [20], to find the concave region of $\widetilde{R}_i^L$ we consider $S_i^L$. Next, we provide the regions in which $S_i^L$ is individually concave in $x$, $y$, and $z$. Later, we find out the overall region for individual concavity of $\widetilde{Q}^L \triangleq \sum_{i=1}^N \widetilde{R}_i^L$ in $x$, $y$, and $z$.

### A. Individual Concavity with Respect to x and y

To check the concavity of $S_i^L$ with respect to $x$, the double derivative of $S_i^L$ with respect to $x$ is given by

$$\frac{\partial^2 S_i^L}{\partial x^2} = \mathcal{A}_1^{-\alpha-\frac{5}{2}}\Bigg(\big((y-y_i)^2+z^2\big)\big((2\alpha+1)(\kappa-1)z-2\alpha\kappa\sqrt{\mathcal{A}_1}\big) - 2(2\alpha+1)(x-x_i)^2\big((\alpha+1)(\kappa-1)z-\alpha\kappa\sqrt{\mathcal{A}_1}\big)\Bigg). \quad \text{(B.1)}$$

On solving $\frac{\partial^2 S_i^L}{\partial x^2} = 0$, (B.1) reduces to

$$u_1^2u_5^2-4u_3^2u_5^3 = (x-x_i)^2\big(2u_1u_2u_4u_5-4u_3^2u_4u_5^2+4u_3^2u_5^2\big) + (x-x_i)^4\big(-u_2^2u_4^2+u_3^2u_4^2u_5-4u_3^2u_4u_5\big)+u_3^2u_4^2(x-x_i)^6, \quad \text{(B.2)}$$

where $u_1 = (2\alpha+1)(\kappa-1)z$, $u_2 = (\alpha+1)(\kappa-1)z$, $u_3 = \alpha\kappa$, $u_4 = 2(1+2\alpha)$, and $u_5 = ((y-y_i)^2+z^2)$. Substituting $w = (x-x_i)^2$ in (B.2), (B.2) reduces to a cubic linear equation with variable $w$ and is given by

$$w^3u_3^2u_4^2+w^2\big(-u_2^2u_4^2+u_3^2u_4^2u_5-4u_3^2u_4u_5\big)+ w\big(2u_1u_2u_4u_5-4u_3^2u_4u_5^2+4u_3^2u_5^2\big) = u_1^2u_5^2-4u_3^2u_5^3. \quad \text{(B.3)}$$

Next, we find the roots of the cubic equation. Since $w = (x-x_i)^2$, we will obtain six roots which divides the search range into seven intervals. Out of seven, we will find the intervals where $\frac{\partial^2 S_i^L}{\partial x^2} < 0$. On solving, we get the overall range where $\frac{\partial^2 S_i^L}{\partial x^2} < 0$. That is $S_i^L$ is concave over the domain $x$ is given by $\mathcal{R}_{xl}^i$ defined by $x \in (-\sqrt{\gamma_3}+x_i, \sqrt{\gamma_3}+x_i)$ given $(y,z)$. The closed form expression for $\gamma_3$ is defined in (B.4), where $q_1 = u_4^2u_3^2$, $q_2 = u_4^2u_5u_3^2 - u_2^2u_4^2 - 4u_4u_5u_3^2$, $q_3 = 4u_5^2u_3^2-4u_4u_5^2u_3^2+2u_1u_5u_2u_4$, and $q_4 = u_1^2u_5^2-4u_5^3u_3^2$.

Since in $S_i^L$, the behaviour of $y$ is similar to $x$, then the region for $x$ is also applicable for $y$. To find the region of $y$, except $u_5 = ((x-x_i)^2+z^2)$, rest all the variable will remain the same and we will form the cubic equation in $w = (y-y_i)^2$. The individual concave region where the function is concave in $y$ is given by $\mathcal{R}_{yl}^i$ defined by $y \in (-\sqrt{\gamma_3}+y_i, \sqrt{\gamma_3}+y_i)$ for a given $(x,z)$. Note that $\mathcal{R}_{xl}^i$, and $\mathcal{R}_{yl}^i$ denote the individual concave regions for $\widetilde{R}_i^L$.

### B. Concavity With Respect to $z$

The double derivative of $S_i^L$ with respect to $z$ is given by

$$\frac{\partial^2 S_i^L}{\partial z^2}=\mathcal{A}_1^{-\alpha-\frac{5}{2}}\big(-2\alpha(2\alpha+1)z^2\big((\kappa-1)z-\kappa\sqrt{\mathcal{A}_1}+((x-x_i)^2 + (y-yi)^2\big)\big(3(2\alpha+1)(\kappa-1)z-2\alpha\kappa\sqrt{\mathcal{A}_1}\big)\big)\big). \quad \text{(B.5)}$$

Simplifying $\frac{\partial^2 S_i^L}{\partial z^2}=0$, (B.5) reduces to

$$z^6\big(4\alpha^2u_1^2(\kappa-1)^2-4\alpha^2u_1^2\kappa^2\big)+z^4\big(-4\alpha^2u_1f_2\kappa^2 + 8\alpha^2f_2\kappa^2-12\alpha u_3f_2(\kappa-1)\big)-4\alpha^2u_2^3\kappa^2+ z^2\big(-4\alpha^2u_2^2\kappa^2+8\alpha^2u_2f_2\kappa^2+9f_1^2\big)=0, \quad \text{(B.6)}$$

where $u_1=1+2\alpha$, $u_2=(x-x_i)^2+(y-y_i)^2$, $u_3=(1+2\alpha)(-1+\kappa)$, $f_1=u_2u_3$, and $f_2=u_1u_2$. Substituting $w=z^2$ in (B.6) turns it into a cubic linear equation. Since $z>0$, we will get three roots which will divide the whole range into four intervals. We obtain the concave region by taking a value within each interval and computing $\frac{\partial^2 S_i^L}{\partial z^2}$. The interval where the $\frac{\partial^2 S_i^L}{\partial z^2}<0$, is taken as the region where the function is concave. On solving, we obtain the region $\mathcal{R}_{zl}^i$ where $S_i^L$ is individually concave in $z$ is defined as $z\in(0,\sqrt{\gamma_z})$ for a given $(x,y)$. The closed form expression for $\gamma_z$ is shown in (B.4), where $q_1=4\alpha^2u_1^2(-1+\kappa)^2-4\alpha^2u_1^2\kappa^2$, $q_2=8\alpha^2f_2\kappa^2-4\alpha^2u_1f_2\kappa^2-12\alpha f_2u_3(-1+\kappa)$, $q_3=9f_1^2-4\alpha^2u_2^2\kappa^2+8\alpha^2f_2u_2\kappa^2$, and $q_4=9f_1^2-4\alpha^2u_2^2\kappa^2+8\alpha^2f_2u_2\kappa^2$.

Thus, the regions obtained for individual concavity of $\widetilde{R}_i^L$ in $x$, $y$, and $z$ are defined as $\mathcal{R}_{xl}^i$, $\mathcal{R}_{yl}^i$, and $\mathcal{R}_{zl}^i$, respectively. When $N$ users are present, we will obtain $N$ regions each for $x$, $y$, and $z$. Then, the overall region for individual concavity of $\widetilde{Q}^L\triangleq\sum_{i=1}^N\widetilde{R}_i^L$ in $x$, $y$, and $z$ is given as

$$\mathcal{R}_x^L=\bigcap_{i=1}^N\mathcal{R}_{xl}^i,\ \mathcal{R}_y^L=\bigcap_{i=1}^N\mathcal{R}_{yl}^i,\ \text{and}\ \mathcal{R}_z^L=\bigcap_{i=1}^N\mathcal{R}_{zl}^i. \quad \text{(B.7)}$$

## ACKNOWLEDGMENTS

This work has been supported by the Department of Science and Technology under Grant no. DST/INSPIRE/04/2016/001127 and IIT Ropar ISIRD grant under Grant no. 9-362/2018/IITRPR/1590.

## REFERENCES

[1] M. Hua, Y. Wang, C. Li, Y. Huang, and L. Yang, "Energy-efficient optimization for UAV-aided cellular offloading," *IEEE Wireless Commun. Lett.*, vol. 8, no. 3, pp. 769–772, June 2019.

[2] N. Gupta, D. Mishra, and S. Agarwal, "3D-trajectory design for outage minimization in UAV-assisted 5G communication system," in *Proc. IEEE CCNC, Las Vegas, USA*, Jan. 2021, pp. 1–6.

[3] N. Gupta, S. Agarwal, and D. Mishra, "Trajectory design for throughput maximization in UAV-assisted communication system," *IEEE Trans. Green Commun. Networking*, pp. 1–13, June 2021.

[4] M. Mozaffari, W. Saad, M. Bennis, and M. Debbah, "Efficient deployment of multiple unmanned aerial vehicles for optimal wireless coverage," *IEEE Commun. Lett.*, vol. 20, no. 8, pp. 1647–1650, June 2016.

[5] A. Al-Hourani, S. Kandeepan, and S. Lardner, "Optimal LAP altitude for maximum coverage," *IEEE Wireless Commun. Lett.*, vol. 3, no. 6, pp. 569–572, Dec. 2014.

[6] J. Lyu, Y. Zeng, R. Zhang, and T. J. Lim, "Placement optimization of UAV-mounted mobile base stations," *IEEE Commun. Lett.*, vol. 21, no. 3, pp. 604–607, Mar. 2017.

[7] R. I. Bor-Yaliniz, A. El-Keyi, and H. Yanikomeroglu, "Efficient 3D placement of an aerial base station in next generation cellular networks," in *Proc. IEEE Int. Conf. Commun. (ICC), Kuala Lumpur, Malaysia*, May 2016, pp. 1–5.

[8] X. Zhong, Y. Huo, X. Dong, and Z. Liang, "QoS-compliant 3D deployment optimization strategy for UAV base stations," *IEEE Sys. J.*, pp. 1–9, Aug. 2020.

[9] M. Alzenad, A. El-Keyi, and H. Yanikomeroglu, "3D placement of an unmanned aerial vehicle base station for maximum coverage of users with different QoS requirements," *IEEE Wireless Commun. Lett.*, vol. 7, no. 1, pp. 38–41, Feb. 2018.

[10] H. He, S. Zhang, Y. Zeng, and R. Zhang, "Joint altitude and beamwidth optimization for UAV-enabled multiuser communications," *IEEE Commun. Lett.*, vol. 22, no. 2, pp. 344–347, Nov. 2018.

[11] Z. Xiao, H. Dong, L. Bai, D. O. Wu, and X. Xia, "Unmanned aerial vehicle base station (UAV-BS) deployment with millimeter-wave beamforming," *IEEE Internet of Things J.*, vol. 7, no. 2, pp. 1336–1349, Feb. 2020.

[12] I. Valiulahi and C. Masouros, "Multi-UAV deployment for throughput maximization in the presence of co-channel interference," *IEEE Internet of Things J.*, pp. 1–1, Sep. 2020.

[13] A. Al-Hourani, S. Kandeepan, and A. Jamalipour, "Modeling air-to-ground path loss for low altitude platforms in urban environments," in *Proc. IEEE Global Commun. Conf. (GLOBECOM), Austin, TX USA*, Dec. 2014, pp. 2898–2904.

[14] M. Mozaffari, W. Saad, M. Bennis, and M. Debbah, "Drone small cells in the clouds: Design, deployment and performance analysis," in *Proc. IEEE Global Commun. Conf. (GLOBECOM), San Diego, CA, USA*, Dec. 2015, pp. 1–6.

[15] Y. Zeng, J. Xu, and R. Zhang, "Energy minimization for wireless communication with rotary-wing UAV," *IEEE Trans. Wireless Commun.*, vol. 18, no. 4, pp. 2329–2345, Apr. 2019.

[16] Y. Chang, "N-dimension golden section search: Its variants and limitations," in *Proc. BMEI, Tianjin, China*, Oct. 2009, pp. 1–6.

[17] A. Alsharoa, H. Ghazzai, M. Yuksel, A. Kadri, and A. E. Kamal, "Trajectory optimization for multiple UAVs acting as wireless relays," in *Proc. IEEE Int. Conf. Commun. Workshops (ICC Workshops), Kansas City, USA*, May 2018, pp. 1–6.

[18] Q. Wu, Y. Zeng, and R. Zhang, "Joint trajectory and communication design for multi-UAV enabled wireless networks," *IEEE Trans. Wireless Commun.*, vol. 17, no. 3, pp. 2109–2121, Mar. 2018.

[19] H. Lee, Y. Kim, Y. Han, and C. Y. Park, "Centroid-based movement assisted sensor deployment schemes in wireless sensor networks," in *Proc. in IEEE 70th Veh. Technol. Conf. Fall, Anchorage, AK, USA*, Sep. 2009, pp. 1–5.

[20] S. Boyd and L. Vandenberghe, *Convex optimization*. Cambridge university press, 2004.

$$\{\gamma_3,\gamma_z\}\triangleq-\frac{\big(1+i\sqrt{3}\big)}{6\sqrt[3]{2}q_1}\sqrt[3]{\sqrt{\big(\pm27q_1^2q_4+9q_1q_2q_3-2q_2^3\big)^2+4\big(3q_1q_3-q_2^2\big)^3}\pm27q_1^2q_4+9q_1q_2q_3-2q_2^3} - \frac{q_2}{3q_1}+\frac{\big(1-i\sqrt{3}\big)\big(3q_1q_3-q_2^2\big)}{3\ 2^{2/3}q_1\sqrt[3]{\sqrt{\big(\pm27q_1^2q_4+9q_1q_2q_3-2q_2^3\big)^2+4\big(3q_1q_3-q_2^2\big)^3}\pm27q_1^2q_4+9q_1q_2q_3-2q_2^3}}. \quad \text{(B.4)}$$